

Adsorption of 4-Nitrophenol onto Iron Oxide Bentonite Nanocomposite: Process Optimization, Kinetics, Isotherms and Mechanism

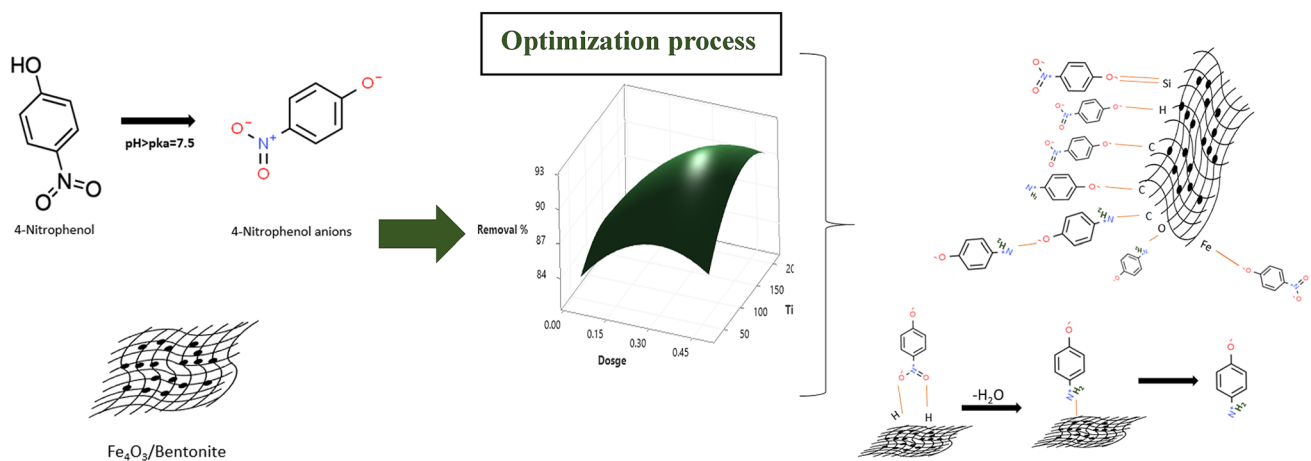
Dina Ewis¹ · Muneer M. Ba-Abbad¹ · Abdelbaki Benamor¹ · Nafis Mahmud¹ · Mustafa Nasser¹ · Muftah El-Naas¹ · Abdul Wahab Mohammad^{2,3}

Received: 24 September 2021 / Revised: 23 January 2022 / Accepted: 12 March 2022 / Published online: 2 April 2022
© The Author(s) 2022

Abstract

Despite its importance in chemical industry, 4-Nitrophenol (4-NP) is a persistent organic pollutant that has serious effects on the ecosystem. In the present study, Box–Behnken design in response surface methodology was used to optimize the adsorption process parameters for the maximum 4-NP removal at 30 °C using Fe₃O₄/Bt NC. The regression model results suggested that the optimum adsorbent dosage, initial concentration, pH and contact time were 0.3182 g, 85 mg/L, 11 and 137.2 min, respectively. The regression model showed an optimum removal of 100%, while 99.5% removal was obtained from batch experiments at the optimum conditions suggested by the regression model, which confirm the model validity. The adsorption data best fitted to Freundlich isotherm model and Pseudo second-order kinetic model suggesting the existence of physical and chemical interaction between the fabricated composite and 4-NP. FTIR analysis suggested that the adsorption mechanism included an electrostatic attraction and the formation of new chemical bonds. Obtained results suggest that Fe₃O₄/Bt NC can be an effective adsorbent for complete 4-NP removal at the indicated optimum conditions.

Graphical Abstract



✉ Muneer M. Ba-Abbad
mbaabbad@qu.edu.qa

Extended author information available on the last page of the article

Article Highlights

- 4-Nitrophenol (4-NP) were successfully removed by synthesized Fe₃O₄/Bt nanocomposite.
- Box-Behnken design in response surface methodology was used to optimize the adsorption process parameters for the maximum 4-NP removal.
- The regression model results suggested that the optimum adsorbent dosage, initial concentration, pH and contact time were 0.3182 g, 85 mg/L, 11 and 137.2 min, respectively.
- The adsorption mechanism of 4-NP as an electrostatic attraction and the formation of new chemical bonds were observed.

Keywords Adsorption · 4-Nitrophenol · Iron oxide · Bentonite · Nanocomposite · Optimization

Introduction

4-Nitrophenol (4-NP) contributes significantly to many industries including dyes (Das and Dey 2020), leathers (Tugba Saka and Tekintas 2020), plastics (Chakraborty 2016) and pharmaceuticals (Wróbel et al. 2000). However, it is a persistent and hazardous organic pollutant with high toxicity and has a serious effect on ecosystem even at very low concentration (Han et al. 2019; Park et al. 2010). 4-NP is considered to be hazardous to human health, aquatic life and plants (Teimouri et al. 2018). Its toxicity can cause health-associated problems to humans such as liver and kidney damage, mouth irritation, blurred vision and systemic poisoning (Fatima et al. 2019; Sellaoui et al. 2019). The continuous ingestion of 4-NP into water and soil requires intensive remediation efforts. This is attributed to the structure stability provided by the nitro group presents in 4-NP, which leads to continuous accumulation of 4-NP in water and soil bodies (Kaur et al. 2019). Therefore, it is considered as a major pollutant by environmental protection Agency (EPA) (Eckenfelder 2000), which specified an allowable maximum NPs concentration levels of 0.01–2.0 µg/L in wastewater streams (Kupeta et al. 2018).

Variety of conventional methods are used to treat 4-NP from wastewater and industrial effluents to meet discharge and environmental regulations, including membrane separation, solvent extraction, chemical oxidation, biological treatment, etc.... However, these technologies are generally associated with high operational cost, time consuming, and formation of other by-products (Ewis et al. 2021; Liu et al. 2020). Adsorption is a simple, feasible, economical and cost-effective method that can significantly reduce the concentration of contaminants, especially with the availability of a wide range of adsorbents with interesting physicochemical properties such as Bentonite clay (Foucaud et al. 2018; Mignon et al. 2020; Saleh et al. 2019; Wadi et al. 2020). Bentonite consists of two silica (SiO₂) tetrahedral sheets with a central alumina oxide (Al₂O₃) octahedral sheet (Nakamura et al. 2020). Furthermore, bentonite is

characterized by several unique physicochemical properties including large specific area, low cost, high porosity, and swelling capability (Gupt et al. 2020; Mudasir et al. 2020). These unique properties endow bentonite with excellent capability to remove water pollutants from aqueous solutions. Kyzioł-Komosińska et al. (Kyzioł-Komosińska et al. 2019), studied the adsorption of Europium (III) ions using bentonite with maximum reported removal efficiency of 99.9% and a maximum adsorption capacity suggested by Sips isotherms model ranged from 2.103 to 77.56 mg/g. However, bentonite still has relatively lower adsorption capability compared to other nanomaterials. Consequently, bentonite can be modified or coupled with other nanomaterials to improve its adsorption capability (Aytas et al. 2009; Lin et al. 2018; Wang et al. 2014). Recently, several authors reported that bentonite supported metal oxides are efficient for water remediation (Babu and Antony 2019; Honarmand et al. 2020; Khatamian et al. 2019; Mishra et al. 2018; Pourshadlou et al. 2020). However, decreased metal oxides particle sizes and the particles aggregation degree are crucial to enhance its adsorption capability (Zhou et al. 2019). The application of Sonochemical during the nanocomposite synthesis can greatly enhance the distribution of metal oxides over the support layer and reduce the metal oxide particle size (Potle et al. 2020) which enhances the adsorption capability of the nanocomposite. Furthermore, the addition of metal oxides with magnetic properties enable nanocomposite separation from aqueous solution (Farooqi et al. 2018).

The aim of this work is to investigate the removal efficiency of 4-NP from wastewater using Iron oxide/Bentonite nanocomposite (Fe₃O₄/Bt. NC) and determine the optimum process parameters using Response Surface Methodology (RSM). RSM has been extensively used to optimize the operational variables for the maximum adsorption capacity, RSM correlates between independent and dependent (response) variables through mathematical and statistical methods (Çelebican et al. 2020). Nevertheless, the literature shows no comprehensive optimization of operational variables for 4-NP maximum removal capacity with any

adsorbent using RSM technique. In this work, Box–Behnken design, which is one of the RSM experimental design techniques, was used for the first time to optimize the experimental parameters of adsorbent dosage, solution pH, solution concentration and contact time. Furthermore, the adsorption isotherms and kinetics data for the removal of 4-NP from wastewater using Iron oxide/Bentonite nanocomposite ($\text{Fe}_3\text{O}_4/\text{Bt. NC}$) were included with a possible mechanism for 4-NP adsorption onto $\text{Fe}_3\text{O}_4/\text{Bt. NC}$ was proposed.

Experimental

Chemical and Materials

4-nitrophenol ($\text{C}_6\text{H}_5\text{NO}_3$) (98%, purity) and ammonia solution 25% (NH_4OH), ferric chloride ($\text{FeCl}_3 \cdot 6\text{H}_2\text{O}$) (99%, purity), ferrous chloride ($\text{FeCl}_2 \cdot 4\text{H}_2\text{O}$) (99%, purity), were purchased from Research Lab fine chem industries.

$\text{Fe}_3\text{O}_4/\text{Bt. NC}$ Synthesis

$\text{Fe}_3\text{O}_4/\text{Bent NC}$ was fabricated by co-precipitation method assisted using ultrasound as reported in our previous work (Ewis et al. 2020). Briefly, 2.5 g of ferrous chloride ($\text{FeCl}_2 \cdot 4\text{H}_2\text{O}$) and 1.5 g of ferric chloride ($\text{FeCl}_3 \cdot 6\text{H}_2\text{O}$) were dissolved in 100 ml of distilled water under nitrogen environment (solution I). Then, 2 g of bentonite was dispersed in 15 ml of ammonia (25%) at 50 °C for 30 min (solution II). After that, solution I was slowly added into solution II and the mixture was stirred for 1 h. The mixture was then placed in an ultrasonic bath for 3 h. Finally, the obtained nanocomposite was separated by a magnet, washed several times with distilled water and ethanol, and dried in a vacuum oven.

Characterization

The characterization of $\text{Fe}_3\text{O}_4/\text{Bent NC}$ including X-ray diffraction (XRD), Transmission Electron Microscopy (TEM), Scanning Electron Microscopy (SEM), Energy Dispersive X-Ray (EDX), Vibrating Sample Magnetometer (VSM) and Fourier-Transform Infrared Spectroscopy (FTIR) were reported in our previous study (Ewis et al. 2020). The surface properties of the nanocomposite after adsorption was investigated by FTIR analyzer over the range 4000–500 cm^{-1} .

Adsorption Study

The adsorption experiments were conducted in a 150 ml Erlenmeyer flask and were continuously stirred in an air bath shaker at 200 rpm and constant temperature of 30 °C

for certain times varying from 30 to 210 min as indicated in Table 4. The solution pH was adjusted as needed using HCl (0.1 mol/L) or NaOH (0.1 mol/L). 4-NP concentration was determined using a concentration-absorbance calibration curve obtained at $\lambda = 317$ nm using a Perkin Elmer Lambda 35 UV/Vis spectrometer. The amount of 4-NP absorbed per unit weight of adsorbent (mg of 4-NP/g of adsorbent) was calculated using Eq. 1:

$$q_e = \frac{C_o - C_e}{m} V \quad (1)$$

where C_o and C_e are the initial and equilibrium concentration of 4-NP (mg/L), V is the solution volume (L), q_e is the equilibrium adsorption capacity and m is the amount of dry mass of nanoparticles added to the solution (g).

The performance of $\text{Fe}_3\text{O}_4/\text{Bent NC}$ for 4-NP removal was account as removal efficiency (RE) using Eq. 2 below.

$$\text{RE}(\%) = \frac{C_o - C_e}{C_o} \times 100\% \quad (2)$$

Statistical Optimization Analysis Using Box–Behnken Design

Batch experiments were designed using Minitab 19 software by implementing Box–Behnken design (BBD) to examine the effect of four indented variables on the response function (adsorption). The BBD experiments involved three levels and four independent variables resulting in 27 experimental runs. The independent variables were adsorbent dosage, initial 4-NP concentration, solution pH and contact time. Table 1 shows the combination of experiments given by BBD for RSM. The relationship between the response and independent variable is demonstrated by second-order

Table 1 Isotherm models' parameters

Isotherm model	Parameter	Value
Freundlich	n	0.499
	K_f ($\text{mg g}^{-1}/(\text{mg L}^{-1})^{1/n}$)	0.0118
	R^2	0.9972
Halsey	n_{th}	0.505
	K_H	0.1105
	R^2	0.9954
Temkin	B (J mol^{-1})	23.067
	A (L g^{-1})	0.06115
	R^2	0.9307
D-R	K_{DR} ($\text{mol}^2 \text{k}^{-1} \text{J}^{-2}$)	$1e^{-7}$
	Q_{DR} (mmol g^{-1})	0.6386
	R^2	0.9876

non-linear quadratic polynomial (Ba-Abbad et al. 2015, 2017) as represented by Eq. 3:

$$Y = \beta_o + \sum_{i=1}^n \beta_i X_i + \sum_{i=1}^{n-1} \sum_{j=i+1}^n \beta_{ij} X_i X_j + \sum_{i=1}^n \beta_{ii} X_i^2 + \varepsilon_i \quad (3)$$

where Y is the response, n is the number of variables and ε is the random error. β_o , β_i , β_{ij} and β_{ii} are the model intercept coefficient, liner effect coefficient, quadratic effect coefficient and interaction effect coefficient, respectively. X_i and X_j are the level of independent variables. The coefficients were determined by least-square regression followed by an analysis of variance (ANOVA). The data were fitted with a quadratic equation and the effect of the process variables on adsorption capacity of $\text{Fe}_3\text{O}_4/\text{Bent NC}$ were observed by RSM.

Results and Discussion

Adsorption Isotherms

Adsorption isotherm studies are important to understand the adsorption mechanism by indicating the interaction type between the adsorbate and the adsorbent (Ewis and Hameed 2021). The adsorption isotherm models for solid–liquid systems are represented by a relationship between the amount of adsorbate adsorbed onto an adsorbent (q_e) and the liquid concentration (C_e) at constant temperature. In this study, Freundlich, Halsey, Temkin and Dubinin–Radushkevitch (D-R) equilibrium isotherm models were employed to fit the adsorption data. Freundlich isotherm model assumes a multilayer adsorption on a heterogeneous surface. The model is described by Eq. 4 (Do 1998).

$$q_e = K_f C_e^{\frac{1}{n}} \quad (4)$$

The linearized form of Freundlich isotherm model is described by Eq. 5.

$$\ln q_e = \ln K_f + \frac{1}{n} \ln C_e \quad (5)$$

where K_f is the adsorption capacity in $(\text{mg g}^{-1})(\text{L mg}^{-1})^{1/n}$ and C_e is the equilibrium concentration in mg L^{-1} , n is an indicator of the adsorption intensity.

Similar to Freundlich model, Halsey isotherm model describes multilayer adsorption on a heterogeneous surface, where the adsorption heat is distributed non-uniformly. In addition, the model evaluates a multilayer adsorption system at relatively large distance from the system. The model is expressed by Eq. 6 (Gholitabar and Tahermansouri 2017).

$$q_e = e^{[\ln K_H - \ln C_e]/n_H} \quad (6)$$

where K_H and n_H are Halsey isotherm constant. The linearized form of Eq. 6 is represented by Eq. 7.

$$\ln q_e = \left(\frac{1}{n_H}\right) \ln K_H - \left(\frac{1}{n_H}\right) \ln C_e \quad (7)$$

Temkin isotherm model (Samarghandi et al. 2009) evaluates the adsorption heat, it assumes that the adsorption heat of all molecules present in a layer decreases linearly due to the increase in surface coverage. Temkin isotherm model is described by Eq. 8.

$$q_e = B \ln(A C_e) \quad (8)$$

where B is related to the adsorbent heat in (J mol^{-1}) and A is the equilibrium-binding constant that corresponds to the maximum binding energy. The model can be linearized and described by Eq. 9.

$$q_e = B \ln A + B \ln C_e \quad (9)$$

D-R isotherm model describes the mechanism of adsorption with Gaussian energy distribution onto heterogeneous surfaces. The model is based on a multilayer adsorption assumption in which it involves Van Der Waal's forces (Günay et al. 2007). The model is described by Eq. 10.

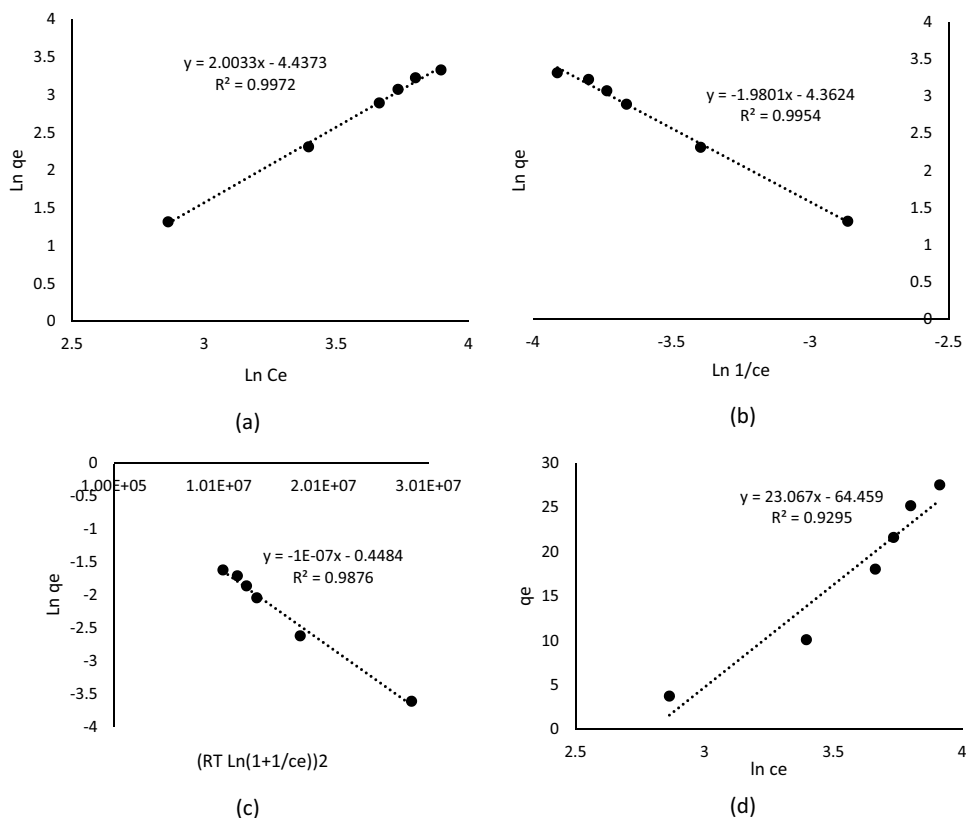
$$q_e = Q_{DR} \exp\left(-K_{DR} \left[RT \ln\left(1 + \frac{1}{C_e}\right)\right]^2\right) \quad (10)$$

where q_e is the amount adsorbed in mmol g^{-1} , Q_{DR} is the maximum adsorption capacity in mmol g^{-1} and K_{DR} is the Dubinin–Radushkevich isotherm constant in $\text{mol}^2 \text{K}^{-1} \text{J}^{-2}$. The model can be linearized and expressed by Eq. 11.

$$\ln q_e = \ln Q_{DR} - K_{DR} \left[RT \ln\left(1 + \frac{1}{C_e}\right)\right]^2 \quad (11)$$

Batch adsorption experiments were carried out for 90 min at pH 5 and adsorbent dosage of 0.1 g at 30 °C. The linearized plots of the mentioned isotherm models are shown in Fig. 1 with the characteristics parameters of each model represented in Table 1. Based on the obtained data, Freundlich model best described the adsorption data with regression coefficient (R^2) equals 0.9972. From mathematical point of view, Freundlich model assumes that the surface coverage goes to infinity; therefore, the saturation of $\text{Fe}_3\text{O}_4/\text{Bent NC}$ with 4-NP cannot be evaluated. Nevertheless, the model can predicts the favorability of the adsorption process by the term n , which is less than 1 indicating that the adsorption process is unfavorable rendering it uneconomical as higher partial pressure is needed to achieve economic adsorption (McCabe and Smith 1967). Halsey isotherm

Fig. 1 Isotherm models **a**: Freundlich model, **b**: Halsey model, **c**: D-R model, **d**: Temkin model



model of adsorption data is fitted as second model with R^2 equals 0.9954, which confirms a multilayer adsorption on a heterogeneous surface. In addition, the model confirms that the adsorption process is unfavorable since n_{th} term 0.505, which sustains the conclusion obtained from Freundlich model. D-R model fitted the adsorption data with R^2 value equals 0.9876. The model shows that the maximum adsorption capacity equals $0.6386 \text{ mmol g}^{-1}$, which corresponds to 88.77 mg g^{-1} . The obtained model parameters were used to determine mean free energy ($E = 1/\sqrt{2K_{DR}}$), found to be equals to 2236 J mol^{-1} . The value of E which is less than 8000 J mol^{-1} indicates a physical adsorption process (Caetano et al. 2009). Finally, Temkin isotherm model fitted the adsorption data with R^2 equals 0.9307. Based on the results obtained, adsorption of 4-NP onto $\text{Fe}_3\text{O}_4/\text{Bent NC}$ was best described by Freundlich model suggesting a non-ideal multiplayer adsorption process on a heterogeneous surface.

To verify the synthesis of $\text{Fe}_3\text{O}_4/\text{Bent NC}$, the adsorption of 4-NP onto raw bentonite was estimated under the same experiment conditions. The experiment was carried out using 0.1 g of adsorbent, pH 5, and 4NP concentration of 100 ppm for 90 min at 30°C . The results showed that raw bentonite attains around 29% removal, whereas $\text{Fe}_3\text{O}_4/\text{Bent NC}$ attains around 53.12%.

Adsorption Kinetics

The adsorption kinetics indicate the rate at which the adsorbent uptake the adsorbate. Pseudo first order (PFO) (Yuh-Shan 2004), pseudo-second order (PSO) (Ho and McKay 1998), and intra-particle diffusion (IPD) (Weber & Morris, 1963) models were used to interpret the adsorption kinetics. PFO shows proportional relationship between adsorption rate and the active sites number, while PSO is based on the adsorption equilibrium capacity. The linear forms of PFO and PSO models are described by Eqs. 12 and 13, respectively.

$$\ln(q_e - q_t) = \ln(q_e) - k_1 t \tag{12}$$

$$\frac{t}{q_t} = \frac{1}{k_2^2 q_e} + \frac{t}{q_e}, \tag{13}$$

where k_1 , k_2 and t are the first-order rate constant (min^{-1}), second-order rate constant (g/mg min) and time (min), respectively.

IPD model indicates the rate-controlling step involved in the adsorption process. The model is represented by Eq. 14.

$$q_t = K_i \sqrt{t} + C \tag{14}$$

where K_i is the rate constant in ($\text{mg/g min}^{0.5}$).

Fig. 2 The kinetic models of 4-NP adsorbed onto Fe₃O₄/Bent NC using **a** PFO, **b** PSO, **c** IPD models

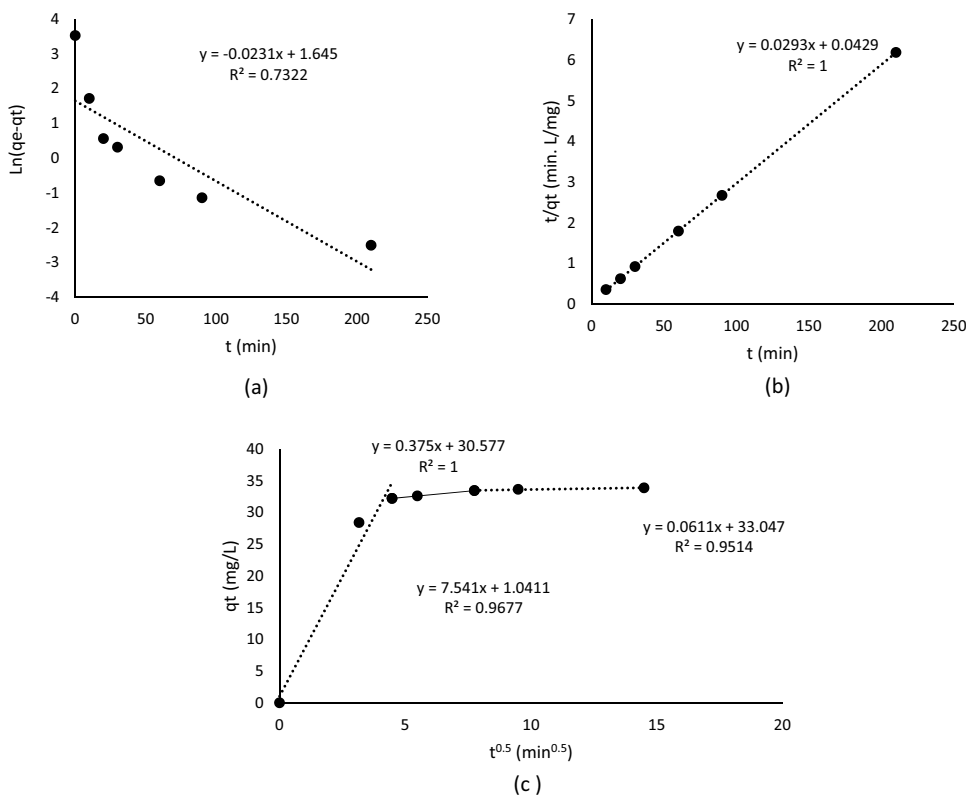


Table 2 Numerical values of the kinetics models parameters

Kinetics model	Parameter	Value
Pseudo first order	Q _e (mg/g)	5.18
	k ₁ (1/min)	0.0231
	R ²	0.7322
Pseudo second order	Q _e (mg/g)	34.13
	k ₂ (g/mg min)	0.0293
	R ²	1.000
Intra-particle diffusion	k _{i1} (mg/g min ^{0.5})	7.541
	k _{i2} (mg/g min ^{0.5})	0.375
	k _{i3} (mg/g min ^{0.5})	0.0611
	C ₁ (mg/g)	1.0411
	C ₂ (mg/g)	30.577
	C ₃ (mg/g)	33.047

Data of batch experiments carried out at 100 ppm solution concentration, pH 5 and adsorbent dosage 0.1 g at a temperature of 30 °C were fitted the kinetic models as shown in Fig. 2. The associated numerical values of the kinetic parameters of each model are presented in Table 2. We can easily observe that the adsorption data did not fit well PFO model with obtained poor R² value equals to 0.7322 (Fig. 2a). In contrast, R² found to be equal to unity (R² = 1.000) for the PSO kinetic model fitting (Fig. 2b) indicating a good fitting. To understand the adsorption mechanism, it is important to

have insights into the rate-controlling step provided by IPD kinetic model shown in Fig. 2c where two complex steps are involved in the adsorption process. The first stage illustrates an instantaneous adsorption characterized by a sharp increase in 4-NP uptake with rate constant k_{i1}. The second stage depicts a gradual increase in 4-NP uptake controlled by intra-particle diffusion with rate constant k_{i2}. The last stage indicates that equilibrium was reached, but an internal diffusion in the pores occurs with rate constant k_{i3}. The numerical values of rate constant shows the rate-limiting step is interior pore-diffusion since k_{i1} is greater than k_{i2} and k_{i3} (Table 2). The constant C in Eq. 14 represents the influence of the boundary layer. The higher C value, the greater is the influence of boundary layer on the adoption process (Hameed 2007). From Fig. 2 c, it is observed that the influence of the boundary layer was significant in the second and the third stages. Furthermore, it can be seen that the C does not attain zero, which confirm the rate-limiting step not including of the intra-particle diffusion.

Box–Behnken Design (BBC) Statistical Analysis

RSM consists of statistical and mathematical techniques, which help to develop models that predict the influence of variables on a response function and optimize the response. BBD was used to optimize the removal of 4-NP using Fe₃O₄/Bent NC by examining the effect of adsorbent dosage,

Table 3 Independent variables range and level

variable	Range and level		
	- 1	0	1
Adsorbent dosage (g)	0.05	0.275	0.5
Initial concentration (ppm)	10	55	100
Solution pH	3	7	11
Contact time (min)	30	120	210

solution initial concentration, solution pH and contact time at fixed temperature of 30 °C. BBD suggested a random order of 27 experiments, which were carried out in duplicates. The level and the range of independent variables are shown in Table 3. The experiments results were processed by the software (Minitab 19) to obtain the theoretical removal. Table 4 shows the 27 experiments suggested by BBD using Minitab 19 with the corresponding actual and predicted removal efficiency. The theoretical removal generated by the software using least-square method is represented by

a quadratic polynomial (Eq. 15), where x_1 is the dosage, x_2 initial concentration, x_3 solution pH, x_4 contact time. A positive sign indicates a synergistic effect of the factors, while the negative sign indicates an antagonistic effect.

$$\begin{aligned}
 \text{Removal\%} = & 54.40 + 49.3x_1 + 0.695x_2 - 1.01x_3 \\
 & + 0.0667x_4 - 54.2x_1x_1 - 0.003032x_2x_2 \\
 & + 0.1780x_3x_3 - 0.000391x_4x_4 - 0.230x_1x_2 \\
 & - 0.47x_1x_3 + 0.0719x_1x_4 - 0.01216x_2x_3 \\
 & + 0.000195x_2x_4 + 0.00011x_3x_4
 \end{aligned} \tag{15}$$

The regression model was evaluated and the ANOVA results are represented in Table 5. The F values and p values determine the significance of each coefficient. The regression model explains well the variation in the response, as the F values are higher. Furthermore, the associated p value determines the statistical significances by estimating if $F_{\text{statistical}}$ is large enough. A p value < 0.05 indicates that the regression model is statistically significant at 95%

Table 4 RSM design matrix and response function values

Run Order	Adsorbent dosage (g)	Initial concentration (ppm)	pH	Contact time (min)	Removal%	
					Actual	Predicted
1	0.05	10	7	120	67.16	67.03208
2	0.5	10	7	120	77.00	77.16968
3	0.05	100	7	120	95.03	93.0032
4	0.5	100	7	120	95.61	93.8258
5	0.275	55	3	30	86.57	88.19211
6	0.275	55	11	30	93.59	93.70947
7	0.275	55	3	210	87.89	88.85586
8	0.275	55	11	210	95.07	94.53162
9	0.05	55	7	30	81.18	84.07484
10	0.5	55	7	30	87.77	86.64299
11	0.05	55	7	210	79.89	81.90584
12	0.5	55	7	210	92.30	90.29789
13	0.275	10	3	120	74.57	72.7136
14	0.275	100	3	120	95.70	98.38898
15	0.275	10	11	120	84.47	82.67192
16	0.275	100	11	120	96.84	99.62378
17	0.05	55	3	120	89.35	85.78416
18	0.5	55	3	120	92.03	92.11026
19	0.05	55	11	120	94.22	92.22672
20	0.5	55	11	120	95.23	96.86082
21	0.275	10	7	30	73.99	72.09593
22	0.275	100	7	30	93.37	91.83005
23	0.275	10	7	210	71.64	71.25938
24	0.275	100	7	210	94.19	94.1525
25	0.275	55	7	120	91.89	91.64137
26	0.275	55	7	120	91.50	91.64137
27	0.275	55	7	120	91.50	91.64137

Table 5 Variance analysis

Source	DF	Adj SS	Adj MS	F value	p value	Re-mark
Model	14	1994.21	142.44	18.19	0.000	Significant
Linear	4	1547.69	386.92	49.42	0.000	Significant
Adsorbent Dosage	1	91.58	91.58	11.70	0.005	Significant
Initial concentration	1	1361.89	1361.89	173.96	0.000	Significant
pH	1	92.52	92.52	11.82	0.005	Significant
Time	1	1.70	1.70	0.22	0.650	Insignificant
Square	4	393.98	98.50	12.58	0.000	Significant
Dosage*Dosage	1	40.10	40.10	5.12	0.043	Significant
Concentration of 4-NP* concentration of 4-NP	1	201.06	201.06	25.68	0.000	Significant
pH*pH	1	43.27	43.27	5.53	0.037	Significant
Time* Time	1	53.43	53.43	6.82	0.023	Significant
2-way interaction	6	52.53	8.76	1.12	0.407	Insignificant
Dosage * 4-NP concentration	1	21.67	21.67	2.77	0.122	Insignificant
Dosage*pH	1	0.70	0.70	0.09	0.770	Insignificant
Dosage*Time	1	8.84	8.84	1.08	0.319	Insignificant
Concentration of 4-NP*pH	1	19.17	19.17	2.45	0.144	Insignificant
Concentration of 4-NP * time	1	2.51	2.51	0.32	0.582	Insignificant
pH* time	1	0.01	0.01	0.00	0.978	Insignificant
Error	12	93.95	7.83			
Lack-of-Fit	10	93.84	9.38	179.98	0.006	
Pure error	2	0.1	0.05			
Total	26	2088.16				

Definition for the significance of [*] is multiplied

confidence level (Mohammad et al. 2019). In this study, the regression model was found to be statistically significant as the F value corresponded to 18.19 with a p value equals to zero (0.000). The determination coefficient (R^2) attained a value of 95.50%, which suggests that the experimental values are in good agreement with the values obtained from the regression model. In addition, the adjusted R^2 was 90.25%, which confirms the statistical significance of the regression model and indicate that the model can be used for further analysis.

The regression model and RSM were used to evaluate the effect of four independent variables on 4-NP adsorption. Figure 3A, B, C, D, E and F shows 3D surface response plots of two factors while keeping other factors constants. Generally, the interaction between all selected variables was insignificant as the p values were higher than 0.05 (Table 5). The 3D surface plot for the optimization of adsorbent dosage with initial solution concentration is shown in Fig. 3A. The figure clearly shows that 4-NP removal increases as the adsorbent dosage and initial solution concentration increased. This could be attributed to the combination effect of active sites availability as the adsorbent dosage rises and an increase in the concentration gradient between bulk solution and the adsorbent as the initial solution concentration increases. The contour plot shown in Fig. 3G indicate that the maximum

removal could be obtained is approximately 95%. Figure 3C shows 3D surface plot for the study effect between the dosage of adsorbent and contact time on 4-NP removal percentage. Generally, the removal of 4-NP increases as the adsorbent dosage and contact time increases. This may be due to the availability of active sites available with adsorption along with the time available that allow more interaction between the adsorbent and 4-NP molecules. As time increases, the vacant sites become occupied and equilibrium is reached. The contour plot shown in Fig. 3I shows that the maximum removal percentage is around 92%. Similar trend is observed for the combined effect of contact time and initial solution concentration on 4-NP removal (Fig. 3F). The contour plot shown in Fig. 3L shows that the maximum removal percentage is around 95%.

The removal of 4-NP using $\text{Fe}_3\text{O}_4/\text{Bent NC}$ is highly pH dependent as can observed from Fig. 3 B, D and E. The figures indicate that the adsorption is maximum under basic conditions. The contour plot shown in figure H and K shows that 96% removal can be obtained at higher dosage and contact time under basic conditions, respectively. In addition, at higher initial solution concentration (e.g. 90 ppm), 4-NP can be completely adsorbed onto $\text{Fe}_3\text{O}_4/\text{Bent NC}$ at a pH of 11 as shown in Fig. 3J.

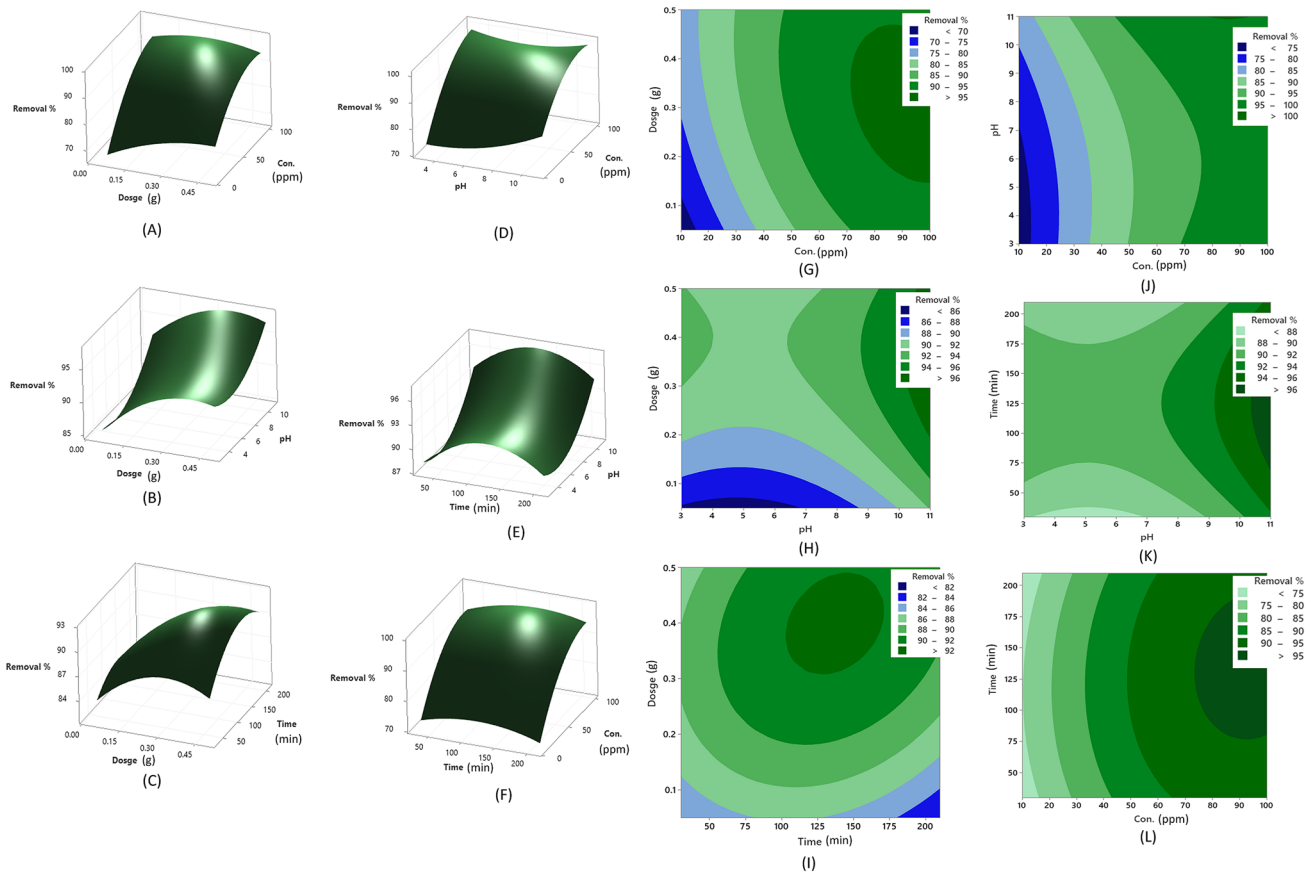


Fig. 3 A–F 3D surface plot G–L contour plots for 4-NP adsorption

Table 6 Optimization solution

Dosage (g)	Initial concentration (mg/L)	pH	Time (min)	Removal % fit	Composite desirability
0.3182	84.5455	11	137.2730	100.00	1

Varying the pH have a significant impact on the adsorption process as it affects Fe₃O₄/Bent NC surface charge and 4-NP degree of ionization. In order, 4-NP have a pka value of 7.15, which means that at a pH lower than 7.15, 4-NP tend to stay at on its molecular form. However, at a pH higher than 7.15, 4-NP dissociates onto 4-NP anions form (Dhorabe et al. 2017). The results obtained from RSM suggests that the adsorption is maximum at pH 11. This could be attributed to the availability of 4-NP anions and its reduction products with Fe₃O₄/Bent NC. The mechanism of adsorption is further discussed in "Adsorption Mechanism"

The optimization results by RSM are shown in Table 6 in which 100% is the optimum removal that can be obtained at the indicated values of independent variables. The removal of 4-NP at the optimization solution was verified. The results suggests that around 99.5% of 4-NP was adsorbed onto Fe₃O₄/Bent NC, which confirms the validity of the regression model. Pareto analysis reveals the relative importance of different independent variables by computing the percentage effect of each independent variable on the response. The Pareto analysis (Fig. 4) suggest that initial 4-NP concentration and pH are the most important factors in the adsorption studies.

Adsorption Mechanism

FTIR spectra were performed on Fe₃O₄/Bent NC before and after adsorption to reveal the surface functional group as shown in Fig. 5. The FTIR spectra represented in Fig. 5a shows the presence of –OH and –FeOO– at absorption peak 3604 cm⁻¹ and 1692 cm⁻¹, respectively. In addition, the peak at 1450 cm⁻¹ can be ascribed to the presence of Si–OH and other peak at 1038 cm⁻¹ for Si–O–Si group is investigated. Furthermore, the figure shows the presence of

Fig. 4 Pareto chart for standardized effects

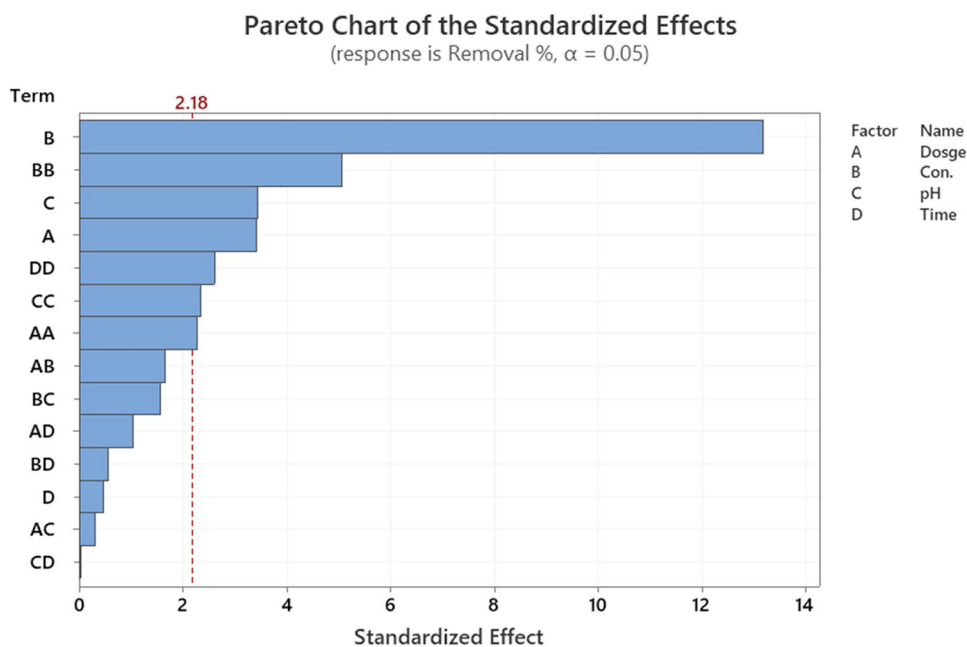
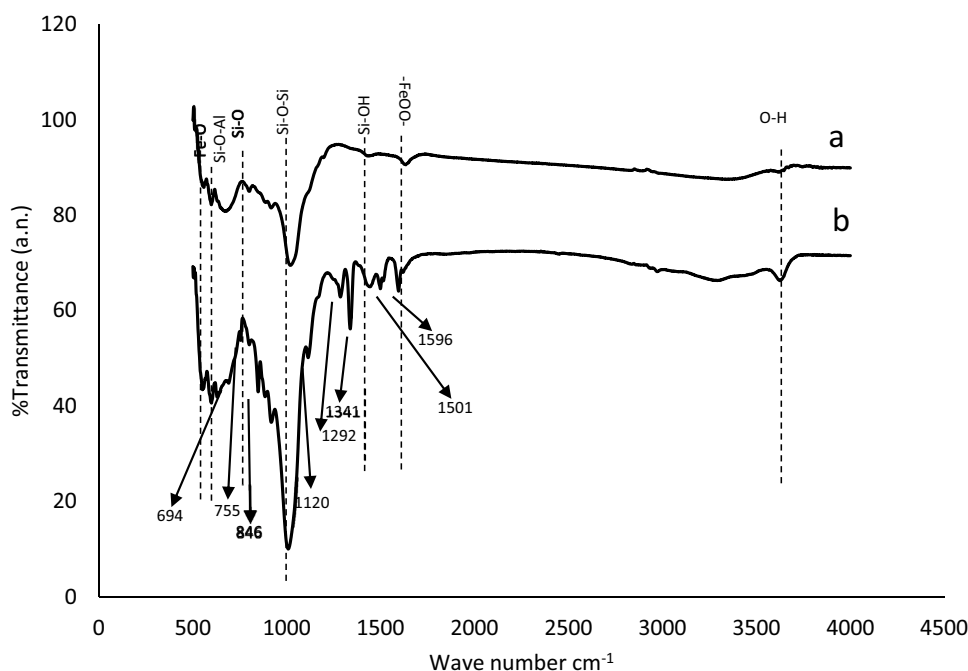


Fig. 5 FTIR spectra **a** before adsorption **b** After adsorption



Si–O, Si–O–Al and Fe–O at the absorption peak 800 cm^{-1} , 609 cm^{-1} and 598 cm^{-1} , respectively. These results confirm the presence and the formation of $\text{Fe}_3\text{O}_4/\text{Bent NC}$. Figure 5b obtained after adsorption, reveals the formation of new peak and increase in few peaks sharpness. As can be seen, the peak sharpness intensity has increased for Si–O, –OH and Si–O–Si groups. The new peaks formed at 755 cm^{-1} and 846 cm^{-1} attributed for C–H group while the peaks at 694 cm^{-1} and 1596 cm^{-1} could be attributed to the presence of C=C. The absorption peak at 1120 cm^{-1} , 1292 cm^{-1} and

1341 cm^{-1} indicate the presence of C–O, C–N and Si=O groups. Finally, the new peak formed at 1501 cm^{-1} could be due to N–O group.

The adsorption mechanism in basic conditions (e.g. $\text{pH} = 11$) is presented in Fig. 6. The adsorption process is expected to occur mainly through van der waals, hydrogen bond, π – π interaction, anion– π interaction, cation– π interaction. As mentioned, 4-NP converts into 4-NP anions when $\text{pH} > \text{pKa}$. Consequently, 4-NP anions interact with $\text{Fe}_3\text{O}_4/\text{Bent NC}$ surface functional groups to form

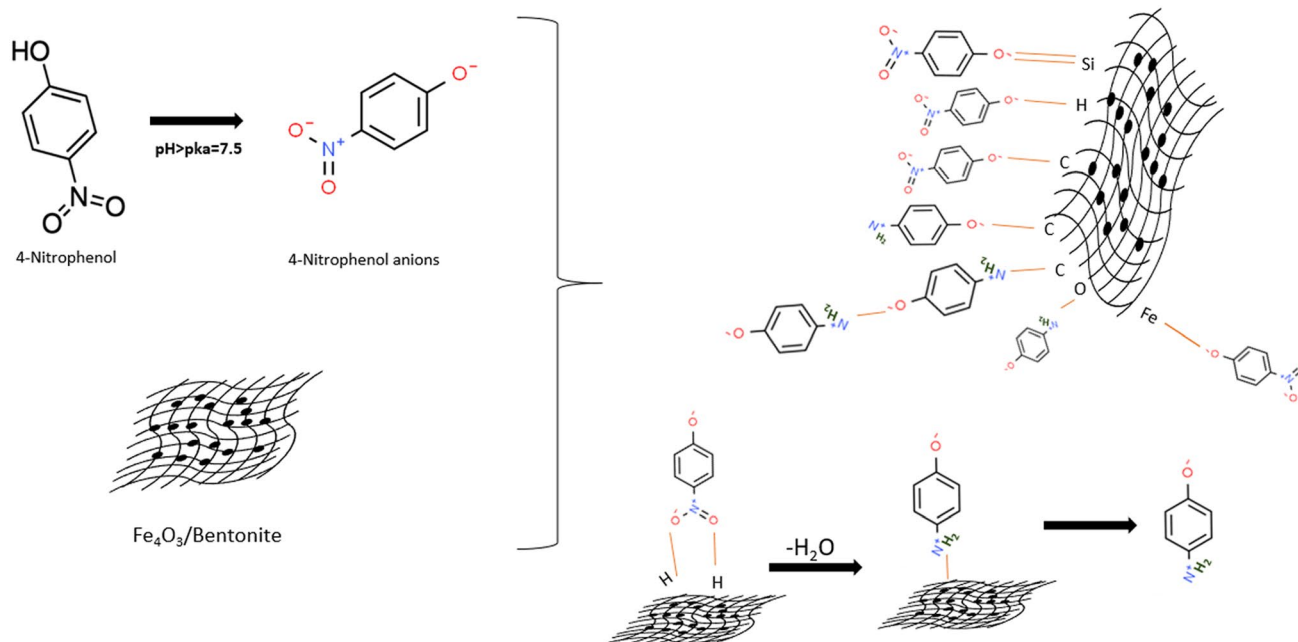


Fig. 6 The mechanism of 4-NP adsorption onto $\text{Fe}_3\text{O}_4/\text{Bent NC}$

chemical bonds. The adsorption kinetics results suggested that the adsorption follows PSO kinetic model, which confirm a chemisorption process. FTIR spectra presented in Fig. 5 confirm the formation of new bond on $\text{Fe}_3\text{O}_4/\text{Bent NC}$ surface after adsorption. Furthermore, the presence of H^+ ions on $\text{Fe}_3\text{O}_4/\text{Bent NC}$ surface, which came originally from aqueous solution cause a redox reaction to produce 4-aminophenol as presented in Fig. 6. This explains the presence of C–N and N–O groups in FTIR spectra (Fig. 5b). The aromatic ring exists in 4-NP contains π electrons which interacts with π electrons exists on $\text{Fe}_3\text{O}_4/\text{Bent NC}$ surface resulting in a strong π – π interaction. The FTIR spectra confirms such interaction by the existence of C=C bond. Furthermore, the bond of O–H indicates a dipole–dipole hydrogen bonding interaction, which is also a type of electrostatic interaction. n – π interaction could be possible interaction, which occur when lone pair of electrons on oxygen delocalize into π orbital of an aromatic ring. In fact, anion– π interaction might be involved in the adsorption process. (Alkorta et al. 2002) studied the interaction between several anions including $[\text{H}]^-$, $[\text{F}]^-$, $[\text{Br}]^-$, $[\text{CN}]^-$ and $[\text{CNO}]^-$ and aromatic ring through Density Functional Theory (DFT) and MPs calculations. The study revealed that these anions interaction favorably with the π cloud of the aromatic ring. In this study, the FTIR spectra revealed the presence of C–N bond, which indicates that anion– π interaction is present. Furthermore, cation– π interaction is also involved in the adsorption process due to the availability of cations including Na^+ and Mg^{+2} (Schottel et al. 2008) mentioned that cations

also interact with π cloud of the aromatic ring. However, the relative strength of cation– π to anion– π interaction strongly depends on the quadrupole moment and the polarizability of the aromatic system. Finally, the EDX results on our previous work revealed the presence on positive ion such as Na^+ and Mg^{+2} (Ewis et al. 2020). Therefore, there could be an electrostatic interaction between negative ions (4-NP, 4-NP anions and 4-aminophenol) and positive ions. In addition, the FTIR spectra prove the presence of electrostatic interaction through Fe–O and Si–O. The isotherm results suggested that adsorption data followed Freundlich isotherm model, which support the presence of physical interaction in the adsorption process.

Conclusion

In this study, the adsorption of 4-NP onto $\text{Fe}_3\text{O}_4/\text{Bent NC}$ was optimized by response surface methodology through Box–Behnken design framework at 30 °C. The optimum conditions of solution pH 11, initial concentration 85 mg/L, contact time of 137.2 min and adsorbent amount of 0.318 g were obtained for 100% 4-NP removal. The maximum removal achieved experimentally was 99.5% under the optimum conditions, which proves the high capability of the studied adsorbent. The regression model results in R^2 value of 95.5%, which proves the model validity. According to the statistical analysis results, 4-NP initial concentration has the most effect on 4-NP adsorption. Furthermore, the adsorption is higher in basic condition

due to the availability of 4-NP anions and 4-aminophenol that are resulted from 4-NP reduction reaction on $\text{Fe}_3\text{O}_4/\text{Bent NC}$ surface. Upon elucidating the mechanism, it is suggested that the adsorption process involves physical and chemical interaction. The process of 4-NP adsorption onto $\text{Fe}_3\text{O}_4/\text{Bent NC}$ was best described by Freundlich isotherm model and PSO kinetic model.

Acknowledgements This research was made possible by an NPRP Grant # 10-0127-170270 from the Qatar National Research Fund (a member of Qatar Foundation). The statements made herein are solely the responsibility of the authors. The author Dina Ewis acknowledged the financial support of QNRF through the Graduate Sponsorship Research Award (GSRA) number GSRA#6-2-0516-19029.

Funding Open Access funding provided by the Qatar National Library.

Declarations

Conflict of Interest On behalf of all authors, the corresponding author states there is no conflict of interest.

Open Access This article is licensed under a Creative Commons Attribution 4.0 International License, which permits use, sharing, adaptation, distribution and reproduction in any medium or format, as long as you give appropriate credit to the original author(s) and the source, provide a link to the Creative Commons licence, and indicate if changes were made. The images or other third party material in this article are included in the article's Creative Commons licence, unless indicated otherwise in a credit line to the material. If material is not included in the article's Creative Commons licence and your intended use is not permitted by statutory regulation or exceeds the permitted use, you will need to obtain permission directly from the copyright holder. To view a copy of this licence, visit <http://creativecommons.org/licenses/by/4.0/>.

References

- Alkorta I, Rozas I, Elguero J (2002) Interaction of anions with perfluoro aromatic compounds. *J Am Chem Soc* 124(29):8593–8598
- Aytas S, Yurtlu M, Donat R (2009) Adsorption characteristic of U(VI) ion onto thermally activated bentonite. *J Hazard Mater* 172(2):667–674
- Ba-Abbad MM, Chai PV, Takriff MS, Benamor A, Mohammad AW (2015) Optimization of nickel oxide nanoparticle synthesis through the sol-gel method using Box-Behnken design. *Mater Des* 86:948–956
- Ba-Abbad MM, Takriff MS, Kadhum AAH, Mohamad AB, Benamor A, Mohammad AW (2017) Solar photocatalytic degradation of 2-chlorophenol with ZnO nanoparticles: optimisation with D-optimal design and study of intermediate mechanisms. *Environ Sci Pollut Res* 24(3):2804–2819
- Babu AT, Antony R (2019) Clay semiconductor hetero-system of SnO₂/bentonite nanocomposites for catalytic degradation of toxic organic wastes. *Appl Clay Sci* 183:105312
- Caetano M, Valderrama C, Farran A, Cortina JL (2009) Phenol removal from aqueous solution by adsorption and ion exchange mechanisms onto polymeric resins. *J Colloid Interface Sci* 338(2):402–409
- Celebicani Ö, İnci İ, Baylan N (2020) Modeling and optimization of formic acid adsorption by multiwall carbon nanotube using response surface methodology. *J Mol Struct* 1203:127312
- Chakraborty B (2016) Kinetic study of degradation of p-nitro phenol by a mixed bacterial culture and its constituent pure strains. *Mater Today Proc* 3(10, Part A):3505–3524
- Das A, Dey A (2020) P-Nitrophenol -Bioremediation using potent Pseudomonas strain from the textile dye industry effluent. *J Environ Chem Eng* 8(4):103830
- Dhorabe PT, Lataye DH, Ingole RS (2017) Adsorptive removal of 4-nitrophenol from aqueous solution by activated carbon prepared from waste orange peels. *J Hazard Toxic Radioact Waste* 21(2):04016015
- Do DD (1998) Adsorption analysis: equilibria and kinetics, vol 2. Imperial college press, London
- Eckenfelder WJ (2000) Industrial water pollution control (McGrawHill)
- Ewis D, Hameed BH (2021) A review on microwave-assisted synthesis of adsorbents and its application in the removal of water pollutants. *J Water Process Eng* 41:102006
- Ewis D, Benamor A, Ba-Abbad MM, Nasser M, El-Naas M, Qiblawey H (2020) Removal of oil content from oil-water emulsions using iron oxide/bentonite nano adsorbents. *J Water Process Eng* 38:101583
- Ewis D, Ismail NA, Hafiz M, Benamor A, Hawari AH (2021) Nanoparticles functionalized ceramic membranes: fabrication, surface modification, and performance. *Environ Sci Pollut Res* 28(10):12256–12281
- Farooqhi A, Sayadi MH, Rezaei MR, Allahresani A (2018) An efficient removal of lead from aqueous solutions using FeNi₃@SiO₂ magnetic nanocomposite. *Surfaces and Interfaces* 10:58–64
- Fatima R, Afridi MN, Kumar V, Lee J, Ali I, Kim K-H et al (2019) Photocatalytic degradation performance of various types of modified TiO₂ against nitrophenols in aqueous systems. *J Clean Prod* 231:899–912
- Foucaud Y, Lebègue S, Filippov L, Filippova I, Badawi M (2018) Molecular insight into fatty acid adsorption on bare and hydrated (111) fluorite surface. *J Phys Chem B* 122(51):12403–12410
- Gholitabar S, Tahermansouri HJCL (2017) Kinetic and multi-parameter isotherm studies of picric acid removal from aqueous solutions by carboxylated multi-walled carbon nanotubes in the presence and absence of ultrasound. *Carbon Lett* 22:14–24
- Günay A, Arslankaya E, Tosun I (2007) Lead removal from aqueous solution by natural and pretreated clinoptilolite: adsorption equilibrium and kinetics. *J Hazard Mater* 146(1-2):362–371
- Gupt CB, Bordoloi S, Sekharan S, Sarmah AK (2020) Adsorption characteristics of Barmer bentonite for hazardous waste containment application. *J Hazard Mater* 396:122594
- Hameed BH (2007) Equilibrium and kinetics studies of 2,4,6-trichlorophenol adsorption onto activated clay. *Colloids Surf A* 307(1-3):45–52
- Han X-W, Bi S, Zhang W, Yang Z (2019) One-step fabrication of highly dispersed Ag nanoparticles decorated N-doped reduced graphene oxide heterogeneous nanostructure for the catalytic reduction of 4-nitrophenol. *Colloids Surf A* 574:69–77
- Ho YS, McKay G (1998) A comparison of chemisorption kinetic models applied to pollutant removal on various sorbents. *Process Saf Environ Prot* 76(4):332–340
- Honarmand M, Golmohammadi M, Naeimi A (2020) Green synthesis of SnO₂-bentonite nanocomposites for the efficient photodegradation of methylene blue and eriochrome black-T. *Mater Chem Phys* 241:122416
- Kaur N, Sood A, Bhasin KK, Kaur G, Bhalla A, Dhau JS et al (2019) Metallosurfactants derived Pd-NiO nanocomposite for remediation of nitrophenol in water. *J Mol Liq* 288:111018
- Khatamian M, Divband B, Shahi R (2019) Ultrasound assisted coprecipitation synthesis of Fe₃O₄/ bentonite nanocomposite:

- performance for nitrate, BOD and COD water treatment. *J Water Process Eng* 31:100870
- Kupeta AJK, Naidoo EB, Ofomaja AE (2018) Kinetics and equilibrium study of 2-nitrophenol adsorption onto polyurethane cross-linked pine cone biomass. *J Clean Prod* 179:191–209
- Kyziol-Komosińska J, Janeczek J, Krzykowski T, Fabiańska MJ, Matuszewska A, Dzieniszewska A et al (2019) Adsorption of Eu(III) onto bentonite and phyllite: a comparative study. *Appl Clay Sci* 183:105330
- Lin J, Jiang B, Zhan Y (2018) Effect of pre-treatment of bentonite with sodium and calcium ions on phosphate adsorption onto zirconium-modified bentonite. *J Environ Manag* 217:183–195
- Liu W, Fan C, Zong Z, Li N, Ma K, Zhu B et al (2020) Two Co(II)-based metal organic frameworks for highly efficient removal of azo dyes from aqueous environment: synthesis, selective adsorption and adsorption mechanism. *Colloids Surf A: Physicochem Eng Asp* 603:125236
- McCabe WL, Smith JC (1967) Unit operations of chemical engineering. McGraw-Hill, New York
- Mignon P, Corbin G, Le Crom S, Marry V, Hao J, Daniel I (2020) Adsorption of nucleotides on clay surfaces: effects of mineral composition, pH and solution salts. *Appl Clay Sci* 190:105544
- Mishra A, Mehta A, Kainth S, Basu S (2018) Effect of g-C₃N₄ loading on TiO₂/Bentonite nanocomposites for efficient heterogeneous photocatalytic degradation of industrial dye under visible light. *J Alloy Compd* 764:406–415
- Mohammad A-T, Abdulhameed AS, Jawad AH (2019) Box-Behnken design to optimize the synthesis of new crosslinked chitosan-glyoxal/TiO₂ nanocomposite: methyl orange adsorption and mechanism studies. *Int J Biol Macromol* 129:98–109
- Mudasir M, Baskara RA, Suratman A, Yunita KS, Perdana R, Puspitasari W (2020) Simultaneous adsorption of Zn(II) and Hg(II) ions on selective adsorbent of dithizone-immobilized bentonite in the presence of Mg(II) ion. *J Environ Chem Eng* 8(4):104002
- Nakamura A, Ozaki M, Murakami K (2020) Elucidation of the aggregation mechanism of bentonite with cationic guar gum as flocculant and application to filtration. *Colloids Surf A* 596:124660
- Park K-H, Balathanigaimani MS, Shim W-G, Lee J-W, Moon H (2010) Adsorption characteristics of phenol on novel corn grain-based activated carbons. *Microporous Mesoporous Mater* 127(1):1–8
- Potle VD, Shirsath SR, Bhanvase BA, Saharan VK (2020) Sonochemical preparation of ternary rGO-ZnO-TiO₂ nanocomposite photocatalyst for efficient degradation of crystal violet dye. *Optik* 208:164555
- Pourshadlou S, Mobasherpour I, Majidian H, Salahi E, Shirani Bidabadi F, Mei C-T et al (2020) Adsorption system for Mg²⁺ removal from aqueous solutions using bentonite/ γ -alumina nanocomposite. *J Colloid Interface Sci* 568:245–254
- Saleh HM, Aglan RF, Mahmoud HH (2019) *Ludwigia stolonifera* for remediation of toxic metals from simulated wastewater. *Chem Ecol* 35(2):164–178
- Samarghandi M, Hadi M, Moayed S, Barjesteh AF (2009) Two-parameter isotherms of methyl orange sorption by pinecone derived activated carbon. *Iran J Environ Health Sci Eng* 6(4):285–294
- Schottel BL, Chifotides HT, Dunbar KR (2008) Anion- π interactions. *Chem Soc Rev* 37(1):68–83. <https://doi.org/10.1039/B614208G>
- Sellaoui L, Kehili M, Lima EC, Thue PS, Bonilla-Petriciolet A, Lamine AB et al (2019) Adsorption of phenol on microwave-assisted activated carbons: modelling and interpretation. *J Mol Liq* 274:309–314
- Teimouri M, Khosravi-Nejad F, Attar F, Saboury AA, Kostova I, Benelli G et al (2018) Gold nanoparticles fabrication by plant extracts: synthesis, characterization, degradation of 4-nitrophenol from industrial wastewater, and insecticidal activity—a review. *J Clean Prod* 184:740–753
- Tugba Saka E, Tekintas K (2020) Light driven photodegradation of 4-nitrophenol with novel Co and Cu phthalocyanine in aqueous media. *J Mol Struct* 1215:128189
- Wadi VS, Mittal H, Fosso-Kankeu E, Jena KK, Alhassan SM (2020) Mercury removal by porous sulfur copolymers: adsorption isotherm and kinetics studies. *Colloids Surf A* 606:125333
- Wang X, Yang L, Zhang J, Wang C, Li Q (2014) Preparation and characterization of chitosan-poly(vinyl alcohol)/bentonite nanocomposites for adsorption of Hg(II) ions. *Chem Eng J* 251:404–412
- Weber WJ, Morris JC (1963) Kinetics of adsorption on carbon from solution. *J Sanit Eng Div* 89(2):31–60
- Wróbel K, Wróbel K, Urbina EMC, Muñoz Romero J (2000) The determination of 3-nitrophenol and some other aromatic impurities in 4-nitrophenol by reversed phase HPLC with peak suppression diode array detection. *J Pharm Biomed Anal* 22(2):295–300
- Yuh-Shan H (2004) Citation review of Lagergren kinetic rate equation on adsorption reactions. *Scientometrics* 59(1):171–177
- Zhou K, Ma W, Zeng Z, Ma X, Xu X, Guo Y et al (2019) Experimental and DFT study on the adsorption of VOCs on activated carbon/metal oxides composites. *Chem Eng J* 372:1122–1133

Authors and Affiliations

Dina Ewis¹ · Muneer M. Ba-Abbad¹  · Abdelbaki Benamor¹ · Nafis Mahmud¹ · Mustafa Nasser¹ · Muftah El-Naas¹ · Abdul Wahab Mohammad^{2,3}

¹ Gas Processing Center, College of Engineering, Qatar University, P.O.Box 2713, Doha, Qatar

² Department of Chemical and Process Engineering, Faculty of Engineering and Built Environment, Universiti Kebangsaan Malaysia, 43600 Bangi, Selangor Darul Ehsan, Malaysia

³ Faculty of Engineering and Built Environment, Centre for Sustainable Process Technology (CESPRO), Universiti Kebangsaan Malaysia, 43600 Bangi, Selangor Darul Ehsan, Malaysia